Revealing a peculiar supernova remnant G106.3+2.7 as a petaelectronvolt proton accelerator with X-ray observations

Chong Ge,[1] Ruo-Yu Liu,[2,3,*] Shu Niu,[4,5] Yang Chen,[2,3] and Xiang-Yu Wang[2,3]

*Correspondence: ryliu@nju.edu.cn

Received: December 16, 2020; Accepted: April 30, 2021; Published Online: May 4, 2021; https://doi.org/10.1016/j.xinn.2021.100118

Graphical abstract

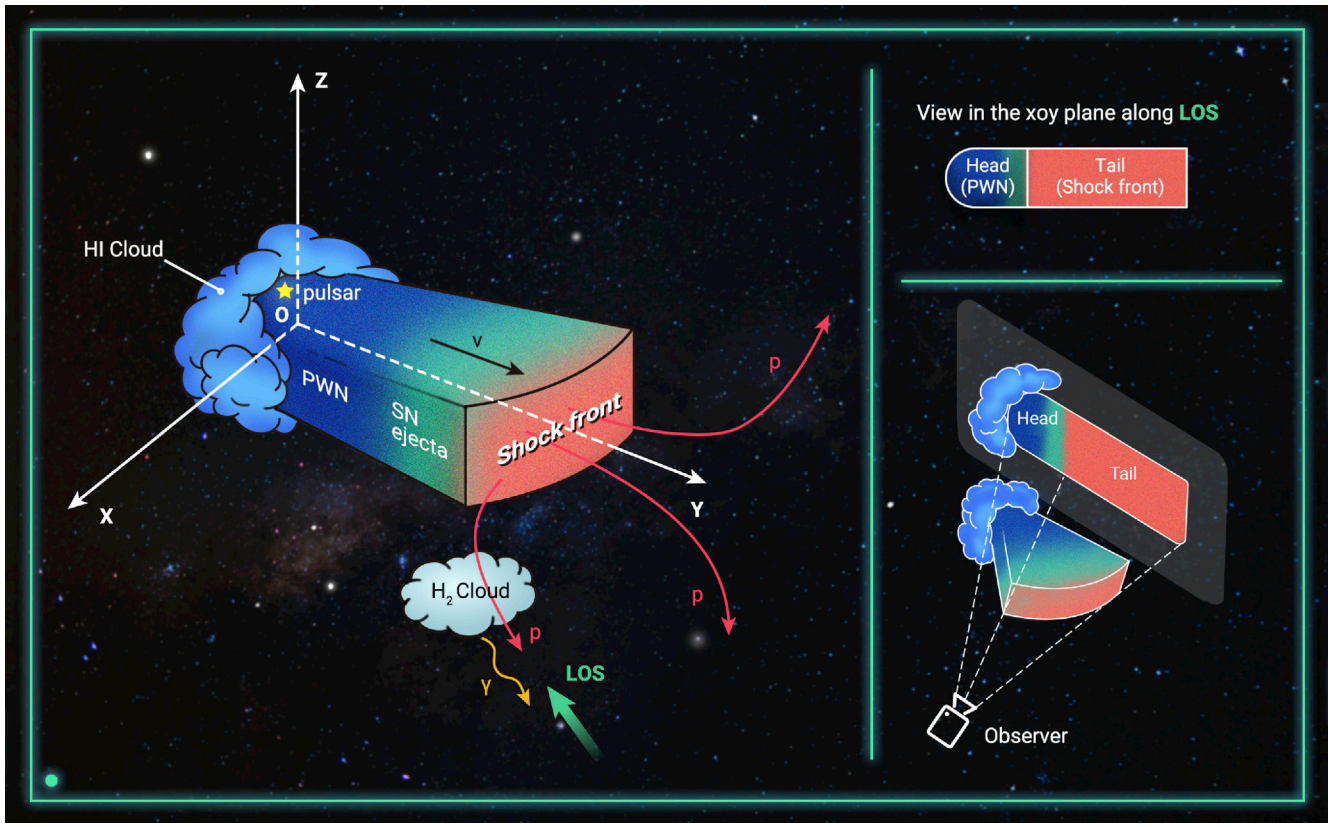

Public summary

- Nonthermal X-ray emission is discovered from the SNR G106.3+2.7
- X-ray observations indicate a high velocity of the SNR shock in the tail region, which is expanding in a low-density hydrogen cavity
- The high shock velocity enables the acceleration of PeV protons, which are also needed to interpret the multiwavelength spectrum of the tail region
- SNR G106.3+2.7 is likely the long-sought source of Galactic PeV cosmic rays

Report

Revealing a peculiar supernova remnant G106.3+2.7 as a petaelectronvolt proton accelerator with X-ray observations

Chong Ge,[1] Ruo-Yu Liu,[2,3,*] Shu Niu,[4,5] Yang Chen,[2,3] and Xiang-Yu Wang[2,3]

[1]Department of Physics and Astronomy, University of Alabama in Huntsville, Huntsville, AL 35899, USA

[2]School of Astronomy and Space Science, Nanjing University, Nanjing 210093, China

[3]Key Laboratory of Modern Astronomy and Astrophysics (Nanjing University), Ministry of Education, Nanjing 210023, China

[4]University of Chinese Academy of Sciences (CAS), Beijing 100049, China

[5]Key Laboratory for Research in Galaxies and Cosmology, Shanghai Astronomical Observatory, CAS, Shanghai 200030, China

*Correspondence: ryliu@nju.edu.cn

Received: December 16, 2020; Accepted: April 30, 2021; Published Online: May 4, 2021; https://doi.org/10.1016/j.xinn.2021.100118

Citation: Ge C., Liu R.-Y., Niu S., et al., (2021). Revealing a peculiar supernova remnant G106.3+2.7 as a petaelectronvolt proton accelerator with X-ray observations. The Innovation **2(2)**, 100118.

Supernova remnants (SNRs) have long been considered as one of the most promising sources of Galactic cosmic rays. In the SNR paradigm, petaelectronvolt (PeV) proton acceleration may only be feasible at the early evolution stage, lasting a few hundred years, when the SNR shock speed is high. While evidence supporting the acceleration of PeV protons in young SNRs has yet to be discovered, X-ray synchrotron emission is an important indicator of fast shock. Here, we report the first discovery of X-ray synchrotron emission from the possibly middle-aged SNR G106.3+2.7, implying that this SNR is still an energetic particle accelerator despite its age. This discovery, along with the ambient environmental information, multiwavelength observation, and theoretical arguments, supports SNR G106.3+2.7 as a likely powerful proton PeV accelerator.

Keywords: cosmic rays; supernova remnants; nonthermal radiation

INTRODUCTION

Cosmic rays (CRs) are high-energy charged particles moving through space at almost the speed of light. They serve as free experimental samples (with a composition of 90% protons, 9% helium nuclei, and 1% heavier elements) to study particle physics and high-energy astrophysics. However, it is impossible to localize the origin of CRs from arrival directions because they are charged particles whose paths have been deflected by magnetic fields intervening between their sources and Earth. Where and how CRs are accelerated remain open questions. The local CR proton spectrum roughly maintains a power law shape up to the so-called knee around 1 PeV (= 10^{15}eV), indicating the existence of powerful proton petaelectronvolt accelerators (PeVatrons) residing in our Galaxy. However, despite decades of efforts, no Galactic sources have been firmly identified as proton PeVatrons except for the indication of a candidate at the Galactic Center.[1] In the supernova remnant (SNR) paradigm of the origin of Galactic CRs, the maximum achievable particle energy is sensitive to the speed of SNR shock. Thus, only SNRs younger than a few hundred years old are considered capable of accelerating PeV protons.[2,3] However, observational evidence has yet to be discovered.

SNR G106.3+2.7 was originally identified in a radio survey of the Galactic plane.[4] As shown in Figure 1, it appears as a cometary structure with a compact "head" of high surface brightness located in the northeastern part of the system and an elongated "tail" of low surface brightness extending toward the southwest.[5] The northern part of the head region is associated with the "Boomerang" pulsar wind nebula (PWN), which is powered by the energetic pulsar PSR J2229+6114 with a high spin-down luminosity of 2.2×10^{37} erg s^{-1}. The pulsar's characteristic age, i.e., 10 kiloyears (kyr), is usually considered as a representation of the system's age,[6,7] although the true age of the pulsar could be younger (Figure S1). The PWN is enveloped by a small H I shell, implying that the PWN is either pushing the H I gas outward or ionizing the atomic hydrogen gas in its vicinity.[8] A dense, shell-like H I structure is also present in the southeastern boundary of the head region, this is likely caused by the encounter of the SNR shock with the dense ambient medium. This scenario is supported by the shell-like enhanced radio emission in the southeastern part of the head region. Based on the central velocity of the H I emission, the distance of the system is considered as $d = 800$ pc,[8] whereas a larger distance is suggested by Halpern et al.[9] In contrast, the tail region appears to be expanding in a low-density hydrogen bubble that may have been excavated by the stellar winds of the previous generation of massive stars.[8]

In the last decade, this region has attracted a lot of attention from the gamma-ray community.[10–15] Milagro detected TeV emission up to 35 TeV with a large spatial uncertainty covering the entire system. VERITAS[12] and Fermi-LAT[13] detected gamma-ray emission in the range of $0.9 - 16$ TeV and $3 - 500$ GeV, respectively, from the tail region. More recently, the HAWC[14] and Tibet ASγ[15] experiments extended the spectrum up to 100 TeV with consistent spatial position of the source from the VERITAS and Fermi-LAT regions as shown in Figure 1. The ASγ data indicate that the measured emission centroid deviates from the pulsar's location, with a confidence level of 3.1σ,[15] although one cannot rule out the possibility that a small fraction of the emission originates from the PWN. Such measurements indicate that very energetic particles are present in the tail region. In principle, both multi-hundred-TeV electrons and PeV protons can produce hundred-TeV gamma-ray photons,[12–16] but the predicted X-ray emission is different in the leptonic and hadronic scenarios.

RESULTS

The Boomerang Nebula is a bright point source surrounded by diffuse emission in the X-ray band with a hard nonthermal spectrum of the photon index 1.5.[9,6] It shows a centrally peaked morphology in the X-ray band, with 29% of the emission coming from PSR J2229+6114. The emission is largely confined within a radius of 100″, spatially coinciding with the shell structure in the radio band, as revealed by an early research[9,6] with ~ 10 ks *Chandra* exposure, as well as by the observations of *ASCA* and *ROSAT*. Currently, the X-ray data from the region of the SNR-PWN complex are much more abundant (summarized in Table S1), with exposure of more than 100 ks by *Chandra*, *XMM-Newton*, and *Suzaku*, respectively.

We analyze the X-ray data from these instruments in the relevant regions as shown in Figure 2 and find the X-ray emission in all the regions of the SNR dominated by a nonthermal component, with a spectrum

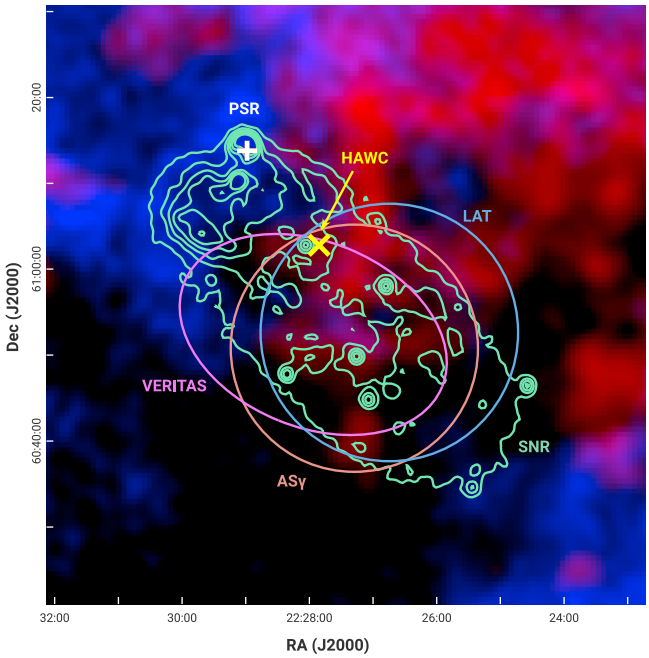

Figure 1. Gas around SNR G106.3+2.7 The blue color represents the distribution of H I gas, and red color shows the CO[8] emission of a dense molecular cloud. The green contours are the 1.4 GHz radio continuum of the SNR. The white plus marks the PSR J2229+6114. The magenta ellipse, cyan circle, and orange circle represent the gamma-ray emission detected by VERITAS, Fermi-LAT, and Tibet ASγ, respectively. The yellow cross shows the best-fit position of the HAWC source. RA and Dec are in J2000.

being consistent with a featureless power law function (see Figure S2 and Table 1). No convincing evidence of line features was identified in the spectral data. The analysis of the Boomerang region in this study (with ten times more *Chandra* exposure) confirms the results of the previous study, and detects fainter nonthermal X-ray emission permeating the entire head region outside the PWN. Similar to the X-ray surface brightness profile (SBP) inside the Boomerang Nebula that is within 100″ from the pulsar, the average radial profile of the extended component in the SNR head decreases with the distance from the pulsar, although in a shallower manner, and is accompanied by a gradual softening of the spectrum. Such features are also observed in other PWNs in the X-ray band,[17–20] suggesting that the extended X-ray emission in the head region is related to the Boomerang Nebula and probably produced by the electrons escaping the PWN. The decline in the X-ray surface brightness and softening in the spectral index are maintained roughly until the boundary between the SNR head and the tail, as shown by the orange dashed arc in Figure 2. They then become constant in the tail region, as measured by *XMM-Newton*. The transition indicates that the X-ray-emitting electrons have a different origin in the tail region compared with those in the head region. Since the X-ray-emitting electrons cool rapidly, these electrons in the tail region should be accelerated *in situ*. The most plausible accelerator in the tail region is the SNR shock. This scenario is corroborated by the fact that a decline in brightness begins immediately outside the northwest boundary of the SNR tail, as shown in Figure 3B (see also the intensity contrast of the TX, TS1, and TS2 regions with the OX1 and OX2 regions in Table 1), demonstrating that fresh X-ray-emitting electrons are produced inside the SNR.

X-ray synchrotron emission has been widely considered as an important indicator of efficient particle acceleration. Previous studies[21–28] have demonstrated that X-ray synchrotron emission only appears in young SNRs (a few thousand years old) in which the SNR shock speed v_s exceeds a few thousand kilometers per second. From a theoretical point of view, the particle acceleration timescale for a particle of energy E (predicted by the diffuse shock acceleration theory[29,30]) strongly depends on the shock speed. It can be estimated by[31,32]

$$t_{\rm acc} \approx \frac{3D}{v_s^2} = \eta^{-1}\left(\frac{r_g}{c}\right)\left(\frac{c}{v_s}\right)^2 \simeq 4\eta^{-1}\left(\frac{E}{1\,\mathrm{TeV}}\right)\left(\frac{B}{10\mu\mathrm{G}}\right)^{-1}\left(\frac{v_s}{3000\,\mathrm{km\ s^{-1}}}\right)^{-2}\mathrm{yr}, \quad \text{(Equation 1)}$$

where $D = \eta^{-1} r_g c/3$ is the spatial diffusion coefficient of the particle, r_g is the particle's Larmor radius, c is the speed of light, B is the magnetic field near the shock front, and $\eta(\leq 1)$ represents the deviation of the diffusion coefficient

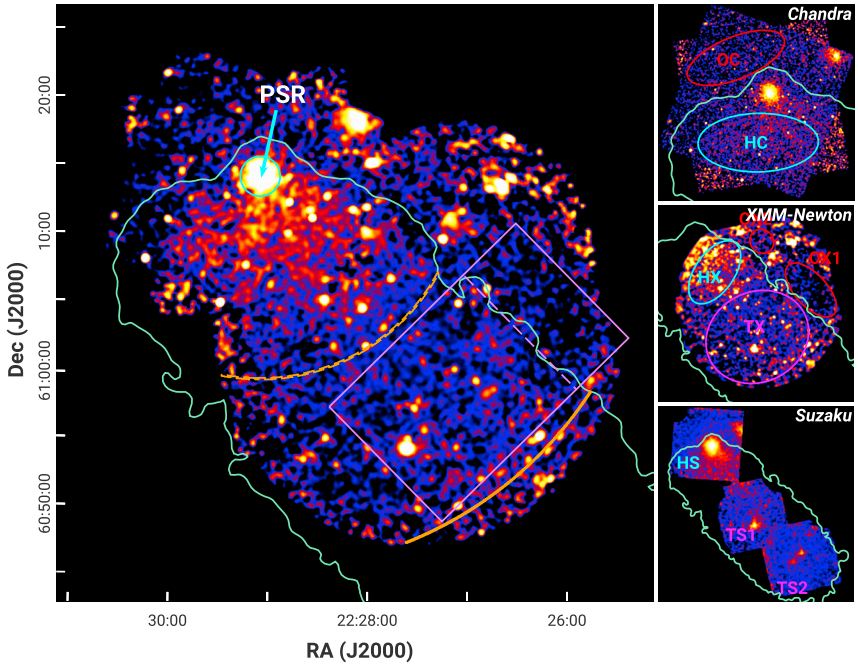

Figure 2. X-ray images of SNR G106.3+2.7 The major panel shows the combined *Chandra* and *XMM-Newton* images in 1–7 keV with instrumental background subtracted and exposure corrected. The green curve outlines the SNR observed by the 1.4 GHz radio continuum.[5] The cyan circle has a radius of 100″ centered at the position of PSR J2229+6114, characterizing the boundary of the Boomerang Nebula. The dashed orange arc marks the approximate boundary between the head and the tail of the SNR in the X-ray band, based on the SBP extracted from a series of annular sectors centered at PSR J2229+6114 out to the position marked with the solid orange arc (see Figure 3A). The magenta box is the intensity extraction region that shows the brightness change at the boundary of the SNR (see Figure 3B). The three small panels show, respectively, *Chandra*, *XMM-Newton*, and *Suzaku* images in 1–7 keV with marked regions for spectral analysis in Table 1. H is short for the head, T is for the tail, and O is for outside the SNR; C is for *Chandra*, X is for *XMM-Newton*, and S is for *Suzaku*. The same green contour outlines the SNR.

Table 1. Spectral properties in different regions of SNR G106.3+2.7

Reg[a]	Power law index	Intensity[b] (erg cm^{-2} s^{-1} arcmin^{-2})	χ^2/DOF
PWN	1.7 ± 0.1	(1.1 ± 0.1) × 10^{-13}	307.6/303
HC	1.9 ± 0.1	(1.3 ± 0.1) × 10^{-14}	734.9/606
HX	2.2 ± 0.1	(1.3 ± 0.1) × 10^{-14}	230.7/192
HS	2.0 ± 0.1	(1.2 ± 0.1) × 10^{-14}	207.6/240
TX	2.4 ± 0.1	(5.4 ± 0.5) × 10^{-15}	1122.0/892
TS1	2.0 ± 0.1	(7.2 ± 0.4) × 10^{-15}	98.8/113
TS2	2.0 ± 0.1	(5.7 ± 0.3) × 10^{-15}	181.5/166
OC	2.6 ± 0.5	(1.3 ± 0.9) × 10^{-15}	399.6/364
OX1	4.5 ± 0.7	(1.0 ± 0.8) × 10^{-15}	224.6/185
OX2	5.8 ± 1.2	(1.9 ± 1.8) × 10^{-15}	156.9/134
BKG	–	(5.6 ± 1.0) × 10^{-15}	–

[a]PWN represents the emission within 100″ of the pulsar but excluding the emission of the pulsar itself. H stands for the head, T for the tail, and O for outside SNR; C stands for *Chandra*, X for *XMM-Newton*, and S for *Suzaku*. The corresponding spectral extraction regions are marked in Figure 2. BKG stands for sky background intensity.
[b]Intensity in 1–7 keV.

from the "Bohm diffusion". This study considers it as the acceleration efficiency. The acceleration of electrons is generally limited by the cooling of synchrotron radiation. Equating the acceleration timescale to the synchrotron cooling timescale, the maximum achievable electron energy in the cooling-limited scenario is obtained and the synchrotron spectral cutoff energy is subsequently derived,[33,34] i.e.,

$$\epsilon_{\rm syn,max} \approx 7\eta \left(v_s/3000{\rm km\ s^{-1}}\right)^2\ {\rm keV}, \qquad \text{(Equation 2)}$$

which is only dependent on the shock speed and η. The continuation of the X-ray spectrum up to 7 keV without a clear spectral cutoff suggests that the SNR shock in the tail region has a high speed, that is $v_s \geq 3000\eta^{-1/2}$km/s.

In general, the inferred high shock speed is unlikely for a middle-aged SNR. However, considering that the tail region is formed by the SNR shock breaking out into a low-density cavity, it is possible that the shock is not significantly decelerated and maintains a high speed. In other words, the SNR in the tail region may not have entered the Sedov-Taylor phase. In addition, the projected length of the tail region is $L_t \simeq 14(d/800\ {\rm pc})$ pc assuming that the supernova explosion center is close to the position of PSR J2229+6114.[8] Therefore, the mean projected shock speed in the tail region can be inferred independently as $v_s \sim L_t/T_{\rm age} \simeq 1500\ {\rm km\ s^{-1}}(d/800\ {\rm pc})(T_{\rm age}/10\ {\rm kyr})^{-1}$. This velocity is generally consistent with the estimate from the X-ray spectrum. Note that the true shock velocity can be several times higher since the velocity inferred in this way is only the component projected on the plane of the sky. In addition, if a shorter age and a larger distance of the system are considered, a larger mean velocity may be obtained.

The high shock speed empowers the tail region to accelerate high-energy protons. Unlike electron acceleration, the proton acceleration is age limited[35] because the energy loss rate of protons is much slower than that of equal-energy electrons. Substituting the formulae for the maximum synchrotron

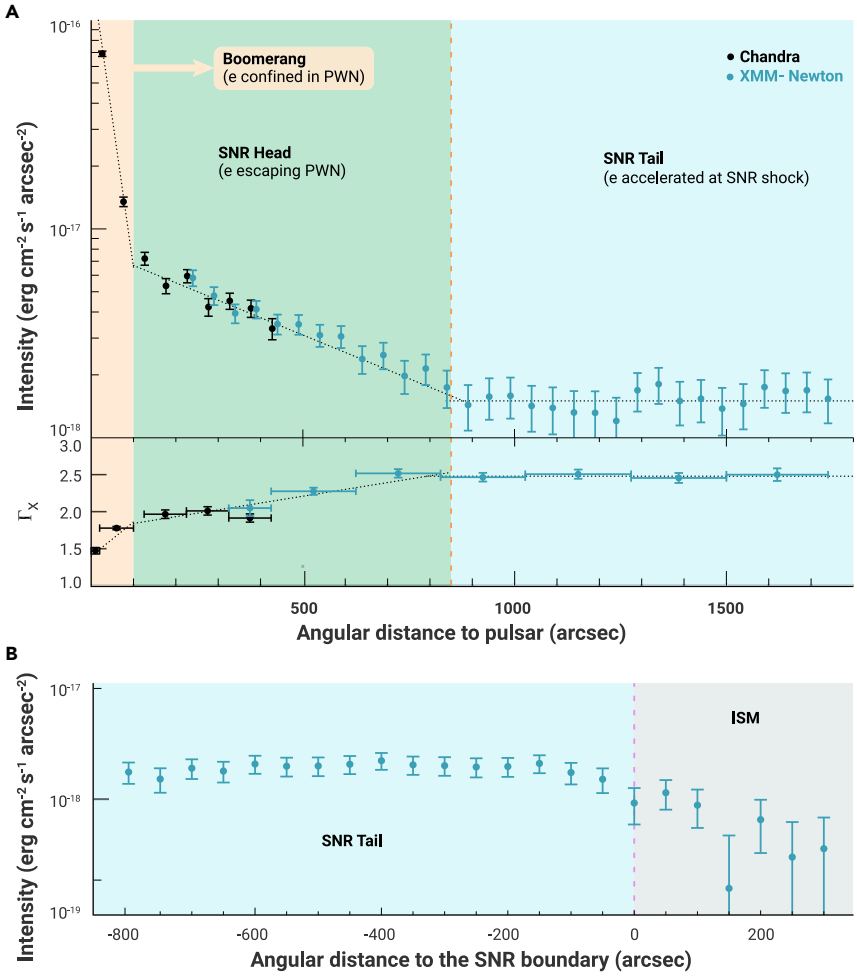

Figure 3. X-ray surface brightness profiles (A) Radial profiles of X-ray surface brightness and the spectral index extracted from a series of annuli centered at PSR J2229+6114. Vertical bars show statistical errors. The central bright point source (i.e., the pulsar's emission) has been subtracted. The three segments of dotted lines represent a PWN component, an escaping electron component in the head region, and an SNR component in the tail region, respectively. The dashed orange line marks the approximate boundary between the head and the tail, corresponding to the position marked with the dashed orange arc in Figure 2.
(B) A one-dimensional X-ray SBP inside the magenta rectangle is shown in Figure 2 after averaging over the short edge of the rectangle. Vertical bars show statistical errors. The dashed magenta line marks the boundary that separates the SNR tail and the interstellar medium (ISM), corresponding to the position marked also with the dashed magenta line in Figure 2.

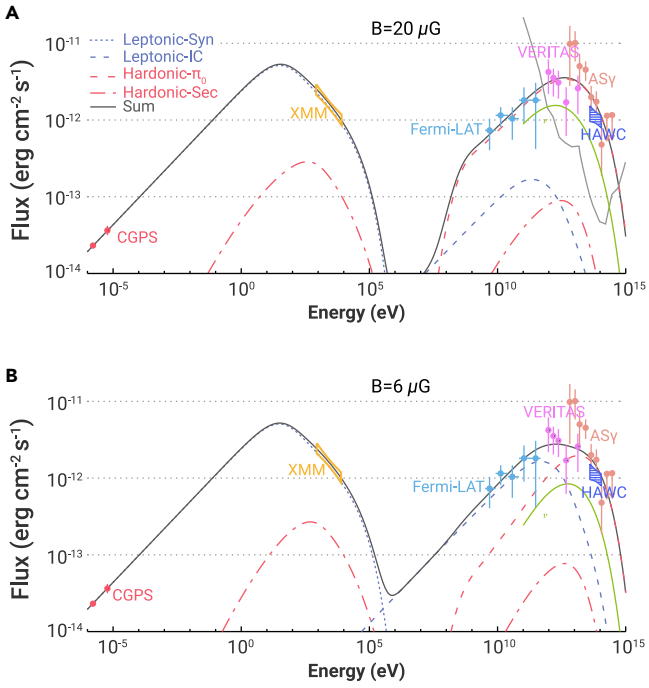

Figure 4. Modeling the spectral energy distribution of the tail region Since the magnetic field is not clearly known, the magnetic fields of B = 20 μG (A) and B = 6 μG (B) are considered. In both panels, the dotted blue curves represent the synchrotron radiation, and the dashed blue curves represent the IC radiation of electrons. The dashed red curves show the pionic gamma-ray emission from *pp* collisions of CR protons while the dot-dashed red curves show the emission of secondary electrons and positrons co-produced in the *pp* collisions. The thick solid black curves show the sum of all these components. The green-yellow curves represent the expected $\nu_\mu + \bar{\nu}_\mu$ flux assuming a flavor ratio of 1:1:1 after oscillation. Model parameters for the case of B = 20 μG: total electron energy $W_e = 3 \times 10^{46}$ergs, electron spectral break energy $E_{e,b}$ = 5 TeV, the maximum electron energy $E_{e,\max}$ = 200 TeV, total proton energy $W_p = 10^{47}$ ergs, proton spectral break energy $E_{p,b}$ = 50 TeV, proton spectral index before the break α_p = 1.7, and the index change after the break $\Delta\alpha_p$ = 0.5. Model parameters for the case of B = 6 μG: $W_e = 2.3 \times 10^{47}$ergs, E_b = 9 TeV, $E_{e,\max} = 400$ TeV, $W_p = 4 \times 10^{46}$ ergs, $E_{p,b}$ = 300 TeV, α_p = 1.6, and $\Delta\alpha_p$ = 0.7. For both these cases, the electron spectral index before the break is α_e = 2.3, the index change after the break is $\Delta\alpha_e$ = 1.4, and the maximum proton energy is $E_{p,\max}$ = 1 PeV. The gas density for the hadronuclear interaction is assumed to be 50cm^{-3}. The CGPS data follow Pineault and Joncas[5]. The Fermi-LAT data was analyzed in Xin et al.[13] The VERITAS data are taken from Acciari et al.[12] and scaled up by a factor of 1.7 to account for the spillover effects.[14] The HAWC data are taken from Albert et al.[14] The Tibet ASγ data are taken from the Tibet ASγ Collaboration.[15] The X-ray bowtie is obtained in this work by multiplying the intensity (flux per solid angle) of the TX region (Table 1) with a solid angle of approximately 600arcmin^2 for the entire tail region. Vertical bars show statistical errors. For reference, the 1-year point source sensitivity of LHAASO[40] is shown with the solid gray curve in (A).

energy $\epsilon_{\rm syn,max}$ or Equation (2) into the formula of the acceleration timescale, the maximum proton energy achievable in the SNR shock of a dynamical age of $T_{\rm age}$ can be given by

$$E_{p,\max} \approx 3\left(\frac{T_{\rm age}}{10\ {\rm kyr}}\right)\left(\frac{B}{10\mu{\rm G}}\right)\left(\frac{\epsilon_{\rm syn,max}}{7\ {\rm keV}}\right)\ {\rm PeV}. \qquad \text{(Equation 3)}$$

In principle, the tail region may serve as a proton PeVatron as long as the magnetic field is not too weak. Generally, the magnetic field in an SNR shock is not expected to be weaker than that in ISM of a typical total strength of 5–10 μG.[36,37]

On the other hand, the spectral energy distribution of the tail region provides information on the magnetic field and even on the necessity of the acceleration of PeV protons in the tail region. In the modeling of the spectrum, d = 800 pc and $T_{\rm age}$ = 10 kyr are employed as the fiducial parameters. For middle-aged SNRs, the emitting electron spectrum is usually given by a broken power law function with a high-energy cut-off.[38,39] We followed this description and found that when the radio and X-ray data in the tail region are well reproduced with the synchrotron radiation of electrons, the gamma-ray spectrum cannot be explained solely by electrons of the same population, and the GeV data disfavor a magnetic field much weaker than B = 6 μG. As shown in Figure 4, the GeV-TeV gamma-ray emission may or may not be reproduced by the inverse Compton (IC) radiation of electrons, depending on the assumed magnetic field. However, the spectrum beyond 30 TeV cannot be interpreted by the IC radiation, because the Klein-Nishina effect suppresses the cross-section of IC scattering at high energies and softens the spectrum (Figure S3).

As a result, a hadronic gamma-ray component that arises from the interactions between accelerated CR protons and gas must be introduced to explain the spectrum of the tail region at least above 10 TeV, because there are no other reasonable particle accelerators in this region. In this scenario, the protons need to be accelerated to 1 PeV or higher to explain the detection of 100 TeV photons. The tail region is spatially coincident with a dense molecular cloud (Figure 1) with an average atom density of 50cm^{-3},[8,14] which can serve as the target for the hadronuclear interactions of CR protons escaping from the SNR. The gamma-ray spectrum can be interpreted well with a proton spectrum of a broken power law with a high-energy exponential cutoff. The spectral break may be caused by the CR confinement in the SNR because lower-energy CRs are more difficult to escape. Therefore, the spectrum becomes harder than the one accelerated at the shock. In contrast, CRs above a certain energy level can more easily escape the SNR, so the spectrum above the break energy is close to the theoretical expectation of shock acceleration with a power law spectral index $\gtrsim$2.[29,30] The required total energy for escaping CRs that are interacting with the molecular cloud is less than 10^{47} ergs. This is reasonable as it constitutes only a tiny fraction of an SNR's energy budget. The flux of co-produced (anti-)muon neutrinos in the hadronuclear interactions would result in a detection of 0.4 track-like events above 50 TeV for the 10-year operation of the IceCube neutrino telescope. This is consistent with the non-detection of neutrino events from the direction of the source.[41]

DISCUSSION

The results of this study indicate that the tail region of SNR G106.3+2.7 is likely a long-sought source of PeV Galactic CRs. Even though it is probably already in the middle-age stage, the nonthermal X-ray radiation from the tail region indicates that its shock velocity still remains at several thousand kilometers per second. This velocity is conducive to the sustained acceleration of protons to PeV energy. The inferred high shock velocity is supported by the expansion of the tail into a low-density cavity. This is consistent with the elongated morphology of the tail. In addition, the multiwavelength spectrum data of the tail region further indicates the necessity of the hadronic component produced by energetic protons with a spectrum extending up to 1 PeV or beyond. This scenario is corroborated by the presence of a dense molecular cloud that spatially coincides with both the tail region and the centroid of the gamma-ray emissions. On the other hand, from a theoretical point of view, SNRs expanding in stellar wind cavities have been suggested as promising accelerators of PeV protons[42,43] because a quasi-perpendicular SNR shock may form in this environment, with an acceleration efficiency comparable with that in the Bohm limit (i.e., $\eta \sim 1$). These various arguments consistently support that the tail region of SNR G106.3+2.7 is likely a Galactic proton PeVatron. In addition to the tail region, the highly asymmetric morphology of the SNR also leaves a clue to study the co-evolution of the SNR-PWN complex system. In-depth theoretical studies on the dynamics, the particle acceleration, and transport processes would facilitate a comprehensive understanding of the system.

SNR G106.3+2.7 is peculiar. To date, it is probably the first and the only middle-aged SNR detected with X-ray synchrotron emission. It is located in a special environment that favors particle acceleration. Its shock velocity is much higher when compared with other middle-aged SNRs, so a high particle acceleration rate is expected. It has experienced a much longer lifetime when compared with young SNRs of fast shock , offering sufficient time for the CRs

to be gradually accelerated up to PeV energies. This discovery challenges the present SNR paradigm of CR origin. In the future, multiwavelength observations by high-performance instruments, such as LHAASO, CTA, and eROSITA will largely promote the discovery and identification of more PeVatrons. Hopefully, these observations will unravel the century-old puzzle of the origin of Galactic CRs.

REFERENCES

1. HESS Collaboration, Abramowski, A., Aharonian, F., et al. (2016). Acceleration of petaelectronvolt protons in the Galactic Centre. Nature ***531***, 476–479.
2. Schure, K.M., and Bell, A.R. (2013). Cosmic ray acceleration in young supernova remnants. Mon. Not. R. Astron. Soc. ***435***, 1174–1185.
3. Bell, A.R. (2015). Cosmic ray origins in supernova blast waves. Mon. Not. R. Astron. Soc. ***447***, 2224–2234.
4. Joncas, G., and Higgs, L.A. (1990). The DRAO galactic-plane survey. II. Field at l = 105. Astron. Astrophys. Suppl. ***82***, 113–144.
5. Pineault, S., and Joncas, G. (2000). G106.3+2.7: a supernova remnant in a late stage of evolution. Astron. J. ***120***, 3218–3225.
6. Halpern, J.P., Camilo, F., Gotthelf, E.V., et al. (2001). PSR J2229+6114: discovery of an energetic young pulsar in the error box of the EGRET source 3EG J2227+6122. Astrophys. J. ***552***, L125–L128.
7. Kothes, R., Reich, W., and Uyanıker, B. (2006). The Boomerang PWN G106.6+2.9 and the magnetic field structure in pulsar wind nebulae. Astrophys. J. ***638***, 225–233.
8. Kothes, R., Uyaniker, B., and Pineault, S. (2001). The supernova remnant G106.3+2.7 and its pulsar-wind nebula: relics of triggered star formation in a complex environment. Astrophys. J. ***560***, 236–243.
9. Halpern, J.P., Gotthelf, E.V., Leighly, K.M., and Helfand, D.J. (2001). A possible X-ray and radio counterpart of the high-energy gamma-ray source 3EG J2227+6122. Astrophys. J. ***547***, 323–333.
10. Abdo, A.A., Allen, B., Berley, D., et al. (2007). TeV gamma-ray sources from a survey of the galactic plane with milagro. Astrophys. J. ***664***, L91–L94.
11. Abdo, A.A., Allen, B.T., Aune, T., et al. (2009). Milagro observations of multi-TeV emission from galactic sources in the fermi bright source list. Astrophys. J. ***700***, L127–L131.
12. Acciari, V.A., Aliu, E., Arlen, T., et al. (2009). Detection of extended VHE gamma ray emission from G106.3+2.7 with veritas. Astrophys. J. ***703***, L6–L9.
13. Xin, Y., Zeng, H., Liu, S., Fan, Y., and Wei, D. (2019). VER J2227+608: a hadronic pevatron pulsar wind nebula? Astrophys. J. ***885***, 162.
14. Albert, A., Alfaro, R., Alvarez, C., et al. (2020). HAWC J2227+610 and its association with G106.3+2.7, a new potential galactic PeVatron. Astrophys. J. ***896***, L29.
15. Tibet ASγ Collaboration, Amenomori, M., Bao, Y.W., et al. (2021). Potential PeVatron supernova remnant G106.3+2.7 seen in the highest-energy gamma rays. Nat. Astron. https://doi.org/10.1038/s41550-020-01294-9.
16. Liu, S., Zeng, H., Xin, Y., and Zhu, H. (2020). Hadronic versus leptonic models for γ-ray emission from VER J2227+608. Astrophys. J. ***897***, L34.
17. Slane, P., Helfand, D.J., van der Swaluw, E., and Murray, S.S. (2004). New constraints on the structure and evolution of the pulsar wind nebula 3C 58. Astrophys. J. ***616***, 403–413.
18. Chen, Y., Wang, Q.D., Gotthelf, E.V., et al. (2006). Chandra ACIS spectroscopy of N157B: a young composite supernova remnant in a superbubble. Astrophys. J. ***651***, 237–249.
19. Tsujimoto, M., Guainazzi, M., Plucinsky, P.P., et al. (2011). Cross-calibration of the X-ray instruments onboard the Chandra, INTEGRAL, RXTE, Suzaku, Swift, and XMM-Newton observatories using G21.5-0.9. Astron. Astrophys. ***525***, A25.
20. Van Etten, A., and Romani, R.W. (2011). Multi-zone modeling of the pulsar wind nebula HESS J1825-137. Astrophys. J. ***742***, 62.
21. Koyama, K., Petre, R., Gotthelf, E.V., et al. (1995). Evidence for shock acceleration of high-energy electrons in the supernova remnant SN1006. Nature ***378***, 255–258.
22. Koyama, K., Kinugasa, K., Matsuzaki, K., et al. (1997). Discovery of non-thermal X-rays from the northwest shell of the new SNR RX J1713.7-3946: the second SN 1006? Publ. Astron. Soc. Jpn. ***49***, L7–L11.
23. Slane, P., Gaensler, B.M., Dame, T.M., et al. (1999). Nonthermal X-ray emission from the shell-type supernova remnant G347.3-0.5. Astrophys. J. ***525***, 357–367.
24. Bamba, A., Koyama, K., and Tomida, H. (2000). Discovery of non-thermal X-rays from the shell of RCW 86. Publ. Astron. Soc. Jpn. ***52***, 1157–L1163.
25. Gotthelf, E.V., Koralesky, B., Rudnick, L., et al. (2001). Chandra detection of the forward and reverse shocks in cassiopeia A. Astrophys. J. ***552***, L39–L43.
26. Hwang, U., Decourchelle, A., Holt, S.S., and Petre, R. (2002). Thermal and nonthermal X-ray emission from the forward shock in Tycho's supernova remnant. Astrophys. J. ***581***, 1101–1115.
27. Reynolds, S.P., Borkowski, K.J., Hwang, U., et al. (2007). A deep Chandra observation of Kepler's supernova remnant: a type Ia event with circumstellar interaction. Astrophys. J. ***668***, L135–L138.
28. Reynolds, S.P., Borkowski, K.J., Green, D.A., et al. (2008). The youngest galactic supernova remnant: G1.9+0.3. Astrophys. J. ***680***, L41.
29. Bell, A.R. (1978). The acceleration of cosmic rays in shock fronts—I. Mon. Not. R. Astron. Soc. ***182***, 147–156.
30. Blandford, R., and Eichler, D. (1987). Particle acceleration at astrophysical shocks: a theory of cosmic ray origin. Phys. Rep. ***154***, 1–75.
31. Kirk, J.G., and Dendy, R.O. (2001). Shock acceleration of cosmic rays—a critical review. J. Phys. G ***27***, 1589–1595.
32. Rieger, F.M., Bosch-Ramon, V., and Duffy, P. (2007). Fermi acceleration in astrophysical jets. Astrophys. Space Sci. ***309***, 119–125.
33. Parizot, E., Marcowith, A., Ballet, J., and Gallant, Y.A. (2006). Observational constraints on energetic particle diffusion in young supernovae remnants: amplified magnetic field and maximum energy. Astron. Astrophys. ***453***, 387–395.
34. Zirakashvili, V.N., and Aharonian, F. (2007). Analytical solutions for energy spectra of electrons accelerated by nonrelativistic shock-waves in shell type supernova remnants. Astron. Astrophys. ***465***, 695–702.
35. Bell, A.R., Schure, K.M., Reville, B., and Giacinti, G. (2013). Cosmic-ray acceleration and escape from supernova remnants. Mon. Not. Roy. Astron. Soc. ***431***, 415–429.
36. Beck, R. (2015). Magnetic fields in spiral galaxies. Astron. Astrophys. Rev. ***24***, 4.
37. Han, J.L. (2017). Observing interstellar and intergalactic magnetic fields. Annu. Rev. Astron. Astrophys. ***55***, 111–157.
38. Ohira, Y., and Yamazaki, R. (2017). Inverse Compton emission from a cosmic-ray precursor in RX J1713.7-3946. J. High Energy Astrophys. ***13***, 17–21.
39. Zhang, X., and Liu, S. (2019). Electron acceleration in middle-age shell-type γ-ray supernova remnants. Astrophys. J. ***876***, 24.
40. Bai, X., Bi, B.Y., Bi, X.J., et al. (2019). The large high altitude air shower observatory (LHAASO) science white paper. arXiv, arXiv:1905.02773.
41. Aartsen, M.G., Ackermann, M., Adams, J., et al. (2020). IceCube search for high-energy neutrino emission from TeV pulsar wind nebulae. Astrophys. J. ***898***, 117.
42. Voelk, H.J., and Biermann, P.L. (1988). Maximum energy of cosmic-ray particles accelerated by supernova remnant shocks in stellar wind cavities. Astrophys. J. ***333***, L65.
43. Zirakashvili, V.N., and Ptuskin, V.S. (2018). Cosmic ray acceleration in magnetic circumstellar bubbles. Astropart. Phys. ***98***, 21–27.

ACKNOWLEDGMENTS

The authors thank all four anonymous referees for their constructive reports. This work is supported by NSFC grant nos. U2031105, 11625312, and 11851304, and the National Key R&D Program of China under grant no. 2018YFA0404203.

AUTHOR CONTRIBUTIONS

R.-Y.L. initiated the project. R.-Y.L. and C.G. wrote the manuscript. C.G. analyzed the *Chandra* and *XMM-Newton* data. S.N. analyzed the *Suzaku* data. R.-Y.L. led the interpretation of the data. Y.C. and X.-Y.W. gave advice on data analysis and theoretical interpretation. All the authors discussed the results and commented on the manuscript.

DECLARATION OF INTERESTS

The authors declare no competing interests.

SUPPLEMENTAL INFORMATION

Supplemental information can be found online at https://doi.org/10.1016/j.xinn.2021.100118.

LEAD CONTACT WEBSITE

Chong Ge: https://orcid.org/0000-0003-0628-5118; Ruo-Yu Liu: https://orcid.org/0000-0003-1576-0961.